Influence of copper plate positioning, zero tool offset, and bed conditions in friction stir welding of dissimilar Al-Cu alloys with different thicknesses

Sachindra Shankar[a], Somnath Chattopadhyaya[a], Kush P. Mehta[b], Pedro Vilaça[c]

[a]*Department of Mechanical Engineering, Indian Institute of Technology, Dhanbad, India*

[b]*Department of Mechanical Engineering, LUT School of Energy Systems, Lappeenranta-Lahti University of Technology (LUT University), Lappeenranta, Finland*

[c]*Department of Mechanical Engineering, School of Engineering, Aalto University, Espoo, Finland*

Corresponding author

Somnath Chattopadhyaya,

Associate professor, Department of Mechanical Engineering, Indian Institute of Technology(ISM), Dhanbad, India

E-mail- somnathchattopadhyaya@iitism.ac.in

Abstract

Friction stir welding of dissimilar thickness aluminium and copper alloys was carried out without offsets by placing the copper at different positions, with horizontal and inclined bed conditions. The influence of the copper plate positions and bed conditions on macro-structure, microstructure, and mechanical properties were investigated. Optical microscopy, FE-SEM, EBSD, Tensile test, bending test, micro-hardness, and XRD analysis were carried out to understand the joint formation mechanism. The joint efficiency of 90% position and 80.08% and bending angles of 93° and 35° were obtained, respectively, when the copper was placed at the middle with horizontal and inclined bed conditions.

Keywords: Friction stir welding, Aluminium alloy, Copper alloy, Horizontal bed, inclined bed, zero offset

1. Introduction

As the modern manufacturing industry grows, traditional monolithic materials frequently fail to satisfy quality demands and thus limiting economic progress. As a result, most industries are

adopting multi-material products that meet the application requirements. Electrical industries are one of them, which uses electrical bus bars in a bulk manner. In the initial days of bus bar design, copper was the metal of choice for design engineers because of its high electrical and thermal conductivity along with good creep and corrosion resistance. But the high cost and weight of copper (Cu) limit its application as a bus bar. On the other hand, aluminium (Al) has better electrical conductivity to weight ratio among all available conducting materials. Although it falls behind copper, because of its higher thermal expansion which is a critical issue at the bolted ends. The modern-day bus bars have passed through many changes, and the current trend is to use Al bus bars with the copper end, which helps in overall weight and cost reduction. Several researchers have already claimed that the bonded or welded joining techniques produce more favourable electrical qualities than force-locking and interlocking procedures when producing electrical contacts.

Fusion welding is one of the most frequent joining processes for various materials. However, because of the considerable differences in melting point temperature and coefficient of thermal expansion, fusion welding presents a challenge while welding dissimilar materials like Al with Cu. Aside from the aforementioned concerns, the formation of large amounts of intermetallic phases during the fusion welding of dissimilar materials is also a major limitation [1][2]. As a replacement, a number of researchers agree that friction stir welding (FSW) is an excellent way to make dissimilar Al–Cu welds [3]. FSW eliminates the limitations of combining these materials with the traditional welding methods by producing joints without visible melting [4]. Initially, FSW was developed for the low melting point temperature materials like Al and Mg [5]. However, FSW is now widely utilized to make high-quality welds in various similar and dissimilar material combinations, including Cu alloys, steel alloys, etc. [6–10]. Additional Methods like post-weld heat treatment can also be utilized to enhance the mechanical property of the different joints[11]. Similarly, interlayer insertion and external cooling and heating sources are also useful techniques during the FSW for the improvement of joint properties [12].

Most of the paper related to FSW of Al and Cu focuses on the placement of Cu or Al along the advancing or retreating side [13], process parameters (such as rotational speed, welding speed, tilt angle, and tool offset) [14–16], pin profiles[17], corrosion properties[18], secondary energy

sources[19][20], intermetallic phases[21], assisted heating and cooling[22] and on the microstructural study[21]. Several researchers claimed that the placement of Cu along the advancing side and Al along the retreating side results in sound joint[23]. Similarly, welds produced with offset result in quality welds, whereas welds produced without offset result in defective welds[15]. Okamura and Aota [24] were among the first to apply this approach to join a range of dissimilar materials and claimed that FSW of Al to Cu or steel is easily possible by inserting most part of the tool pin along Al side . Tool offset is one of the most critical parameters in FSW and has been studied by several researchers in joining dissimilar materials [25]. Hou et al. [26] studied the effect of tool offset on FSW of dissimilar Al6061-T6 and Cu11000 alloys. The results show that higher offsetting of tool towards copper side degraded the surface quality. The maximum strength of 152 MPa was obtained with a tool offset of 1.6 mm. Xue et al. [27] also reported the morphological, structural, and mechanical aspects of 5-mm-thick friction-stir welds between 1060 aluminium and pure copper with tool offsetting towards the aluminium side and without offsets. The researchers experimented with different degrees of offsetting and found that smaller offsetting values (especially 0 mm) resulted in unsatisfactory welds with poor surface finish. Shankar et al. [28] selected different offsets of 1 mm and 0 mm to weld the different thickness Al and Cu and concluded that the welds produced with 1 mm offsets results in improved joint strength compared to the 0 mm offsets.

Tool offsets play a significant role in the friction stir welding of dissimilar materials having completely different properties. In a similar manner, bed condition also play a critical role in the FSW of dissimilar thickness materials. Formation of flash is a critical issue in the friction stir welding of dissimilar thickness materials in horizontal bed conditions, which finally leads to an uneven surface. Tavares et al. [29] welded similar AA2198 plates of 2.5 mm, 3.2 mm, and 4.5 mm thicknesses in horizontal bed conditions and observed thick flash on the weld surface. However, besides the flash formation, no critical issue is reported. Hovanski et al. [30] also mentioned flash formation in the FSW of 1.2 mm and 2 mm thick AA5182-O sheets in horizontal bed conditions. A similar type of flash generation is also observed in the joining of AA1050-H111 sheets of 1.5 mm and 2 mm thickness by Silva et al [31]. In all the above mentioned literatures smaller thickness metal was positioned at the bottom position with respect to the thicker metals. In a similar manner, horizontal bed condition was the most preferred bed condition for different thickness of metals despite the flash formation.

Because Al and Cu have different electrical conductivities, sheet thickness must be adjusted before combining the two materials to maintain a constant current-carrying behavior. However, joining materials with different thicknesses in butt joint configuration is challenging because of the uneven surface level. On the other hand, the lap joint is not a suitable configuration for bus bar design because of the additional material and gap at the joint lead to a higher risk of corrosion. In addition to that, several researchers have attempted to weld the different thickness Al alloys (tailor welded blanks) for various applications in the automotive industry. Fratini et al. [32] joined the two different thickness Al alloys by FSW and obtained a maximum joint efficiency of 80%. Several researchers also studied the formability of tailor welded blanks[33–35]. Besides the similar material, dissimilar materials of different thicknesses are also gaining interest recently. Beygi et al. [36] used the stationary shoulder to weld the dissimilar thickness Al and steel, which led to the seamless joint. Shankar et al. [28] friction stir welded the Al and Cu of different thicknesses by considering different electrical conductivity of the materials.

The current paper deals with the FSW of different thicknesses Al and Cu alloys in which the thickness of Cu is half the thickness of Al alloy. So an attempt has been made to weld dissimilar Al-Cu alloys with different thicknesses by placing the Cu at different positions, i.e., at the top, middle and bottom, with reference to Al alloy. The study also discusses the effect of zero offsets and the formation of flash on the weld quality. In addition to the tilt angle, a new terminology, bed inclination angle, is introduced to investigate the effect of this parameter on joint quality and flash formation

2. Materials and methods

Al alloy AA1050 of 6 mm thickness and oxygen-free copper (Cu-OF-04) of 3 mm thickness were used as a base metal. The chemical composition of each material is mentioned in the table. 1. 160 mm × 95 mm plates of each material were used for the experiments.

Table 1. Chemical composition of base materials

Material	Al	Zn	Mg	Cu	Fe	Si
AA1050	Balance	0.07 wt.%	0.05 wt.%	0.05 wt.%	0.4 wt.%	0.25 wt.%
Cu-OF	O_2 max 10 ppm			99.99 %		

Since Cu is half of the thickness of Al alloy, therefore, a supporting plate of 3 mm and 1.25 mm is required underneath while the Cu is placed at the top and middle positions, respectively. On the other hand, no supporting plate is required when the Cu is placed at the bottom position. Cu was placed along the advancing side for all of the experiments as suggested by several literature. The experiments were performed on a professional FSW machine and weld tool of tempered H13 steel. A concave shoulder tool with a 20 mm diameter and a flat tapered pin was used for all experiments. The probe diameter in the root area was 5 mm, and at the top was 4.2 mm. The length of the pin was 2.9 mm, slightly less than the thickness of Cu to protect the weld from over-penetration. The experiments were repeated three times as per the standard procedure. However, only the best sample for each condition was considered for the analysis, as shown in fig. 2. The process has also shown good repeatability.

Table 2. Condition at which samples were prepared

Sample No		Cu plate position compare to Al	Weld condition (Horizontal/Inclined bed)
S1		Top position	Horizontal bed
S2	Cu — Al	Top position	Inclined bed (4.30˚)
S3		Middle position	Horizontal bed
S4	Cu — Al	Middle position	Inclined bed (4.30˚)
S5		Bottom position	Horizontal bed
S6	Cu — Al	Bottom position	Inclined bed (4.30˚)

The experiments were performed with a fixed rotational speed of 640 rpm, welding speed of 160 mm/min, tool offset of 0 mm, and tilt angle of 2°. These parameters were selected based on the number of trails. All of the experiments were performed on position control mode because of the different joint configuration. Different experiments were conducted by keeping the Cu at different positions, i.e., top, middle, and bottom, as shown in table 2. Two different approaches, horizontal and inclined bed conditions, were used for welding the two alloys while Cu was placed at different positions. Fig. 1 represents the experimental setup in both conditions and the weld tool.
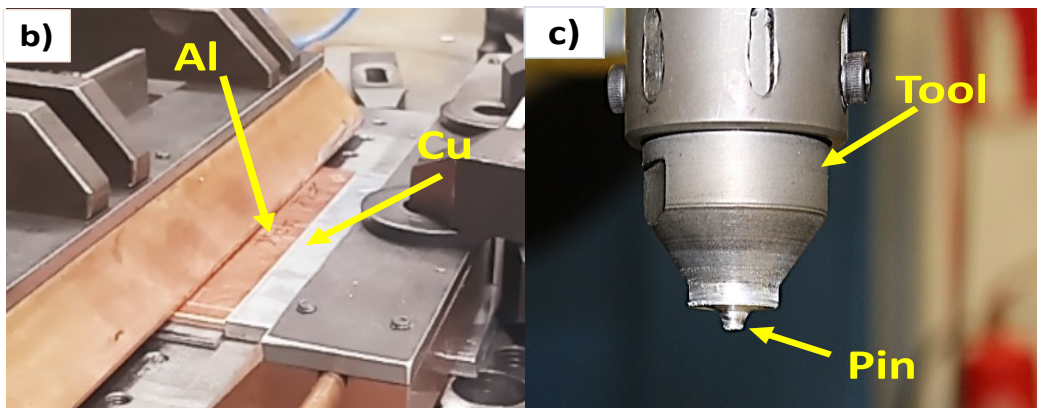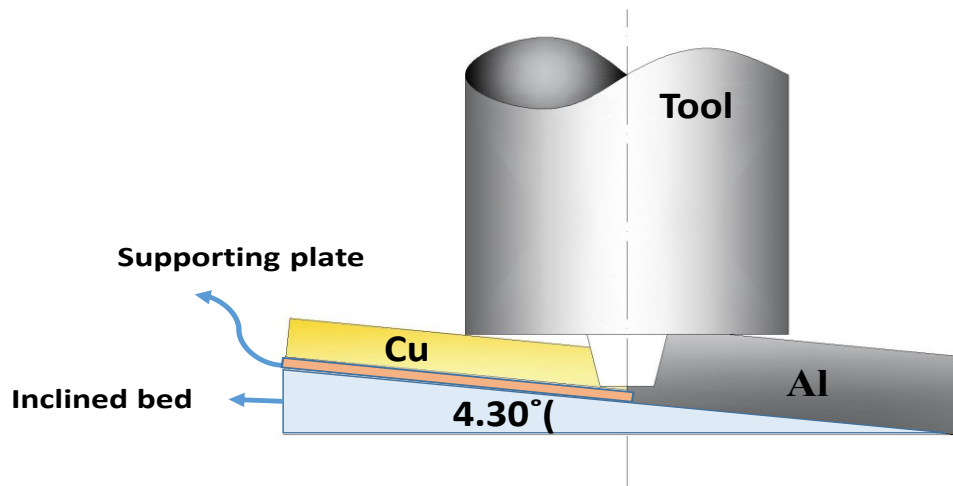
a)

Figure 1 Experimental setup a) inclined bed condition b) Horizontal bed condition c) FSW Tool

Samples for tensile, bending, microstructural, and macro-structural analysis were cut perpendicular to the direction of the weld by a wire EDM machine. The microstructural and EBSD analysis were done on FESEM machine. The transverse tensile tests specimen were cut from the

welded sample, and tests were conducted on a tensile testing machine according to ASTM E8-16a guidelines. X-ray diffraction (XRD) analysis was performed to identify IMCs.

3. Results and discussion

3.1. Surface morphology and cross-sectional analysis

Surface morphologies and cross-sectional observation of the welded samples prepared at different conditions are shown in fig. 2 and 3. The formation of flash is a widespread phenomenon in every weld. Though, it can be seen that in most of the conditions, flash was formed along the Al side, whereas it was shifted toward the Cu side in weld S2. Since Cu was placed on the upper side in the inclined bed, the straight penetration of the tool presses the Cu more than Al and thus results in the formation of Cu flashes which is rare in the other welds comparatively. Except for the samples S1 and S2, all of the samples possess an additional volume of Al in the weld zone due to placement of Cu at the middle and bottom position and thus produces more flashes comparatively. However, this additional volume further eliminates the surface cracks which acts as the failure initiation zone. The cross-sectional profile of each sample is shown in fig. 3 wherein Cu fragments were highlighted. The tunnel or root defect is common in each sample except sample S3. The reason for the root defect in S2 is the lack of Al in the weld zone, whereas the cause for the defect in samples S5 and S6 is an inadequate alignment of the tool shoulder and insufficient force, which keep the material in the weld zone, respectively. In the case of Cu at the bottom position, the inclined bed performs better than the horizontal bed because of the concentrated movement of Al in the weld zone comparatively. The joining mechanism of S5 is the slight diffusion of both materials. It has been concluded from the above discussion that the inclined bed works perfectly for the Cu at the middle and bottom positions due to the aligned shoulder and concentrated force. A horizontal bed, on the other hand, produces the defect-free weld when Cu is positioned in the middle position. The difference in the level of both the materials restricts the complete penetration of the pin in the weld zone and thus reduces the amount of Cu, which further helps in sound and stable weld.
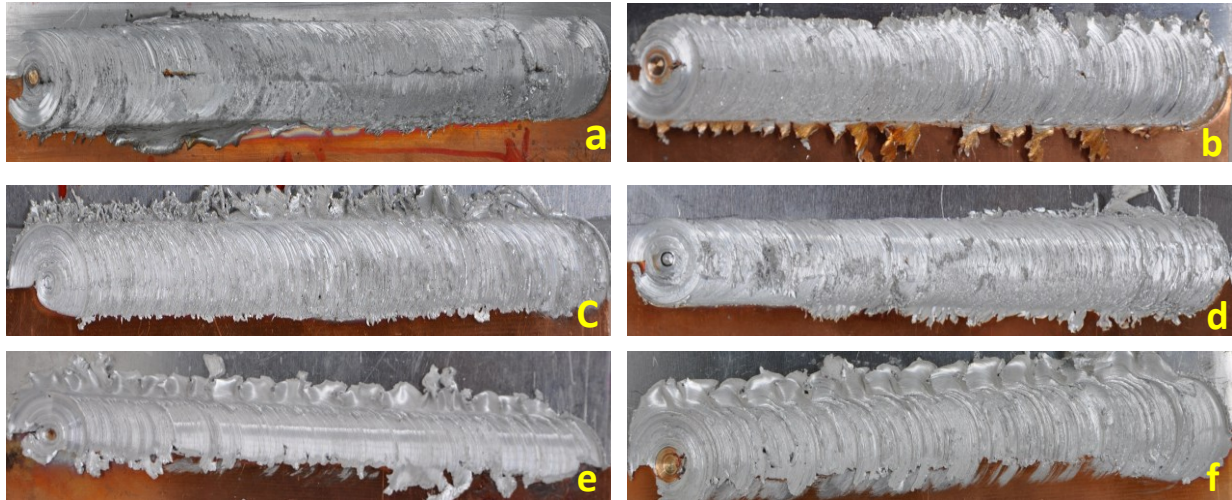
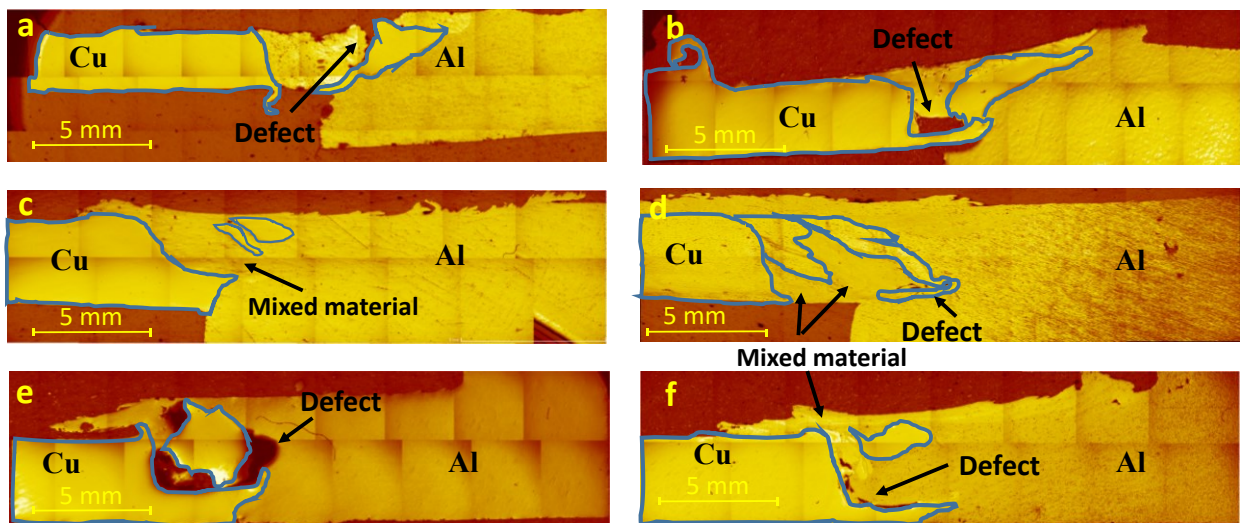*Figure 2 Surface morphologies of a) S1 b) S2 c) S3 d) S4 e) S5 f) S6*

Figure 3 Macro observations of welded samples a) S1 b) S2 c) S3 d) S4 e) S5 f) S6

3.2. Microstructural analysis

Fig. 4 depicts micrograph of welds that reveals the mixing of Al and Cu in the weld zone generated by the stirring effect of the tool. The section examines the various sorts of structures generated by the migration of Al and Cu. Fig 4a and 4b show the macrograph of sample S3 and S4, and fig 4c, 4d, 4e, 4f, 4g, and 4h depicts the microstructure of different region of the samples S3 and S4. It is observed that most of the structures are formed at the bottom of the weld zone. Fig. 4c and 4e represent the composite structure, whereas fig. 4d shows the lamellar type of structure in sample

S3. Fig. 4f displays the lamellar structure in sample S4, at the bottom of the weld zone and near and away from the interface. A large amount of finer and denser Cu material is dispersed in the Al matrix, which forms a composite-like structure and thus results in the strengthening of the joint. The other type of structure is lamellar structures, mainly formed around the onion ring or whirl structure in the bottom area of the weld zone. It should be noted that the lamellar structures are made up of alternate layers of Al and Cu. A similar structure was also reported by Karrar et al. [19]. On the other hand, Liu et al. claimed that the lamellar structure resembles a non-concentric ellipse wherein the curvature of the elliptical layer increases towards the periphery [21]. According to Lee et al., these onion ring and whirl patterns are composed of lamellar-like structures [20]. Besides the composite and layered structure, as depicted in fig 4g, sample S4 also resembles a vortex flow structure at the extreme bottom part of the weld zone along the Al side. Small Cu fragments and Al alloy rotate around the pin and move downwards due to the whirl effect and thus resulting in vortex flow structure at the weld zone bottom [18]. Whereas large Cu particles move out due to their heavy nature and lack of flowability. As demonstrated in fig. 4h, a wavy or S-type pattern is also common in friction stir welding derived from sample S4 at the bottom and near the interface. Wei et al., on the other hand, termed a similar type of pattern as a mixed flow zone [22].
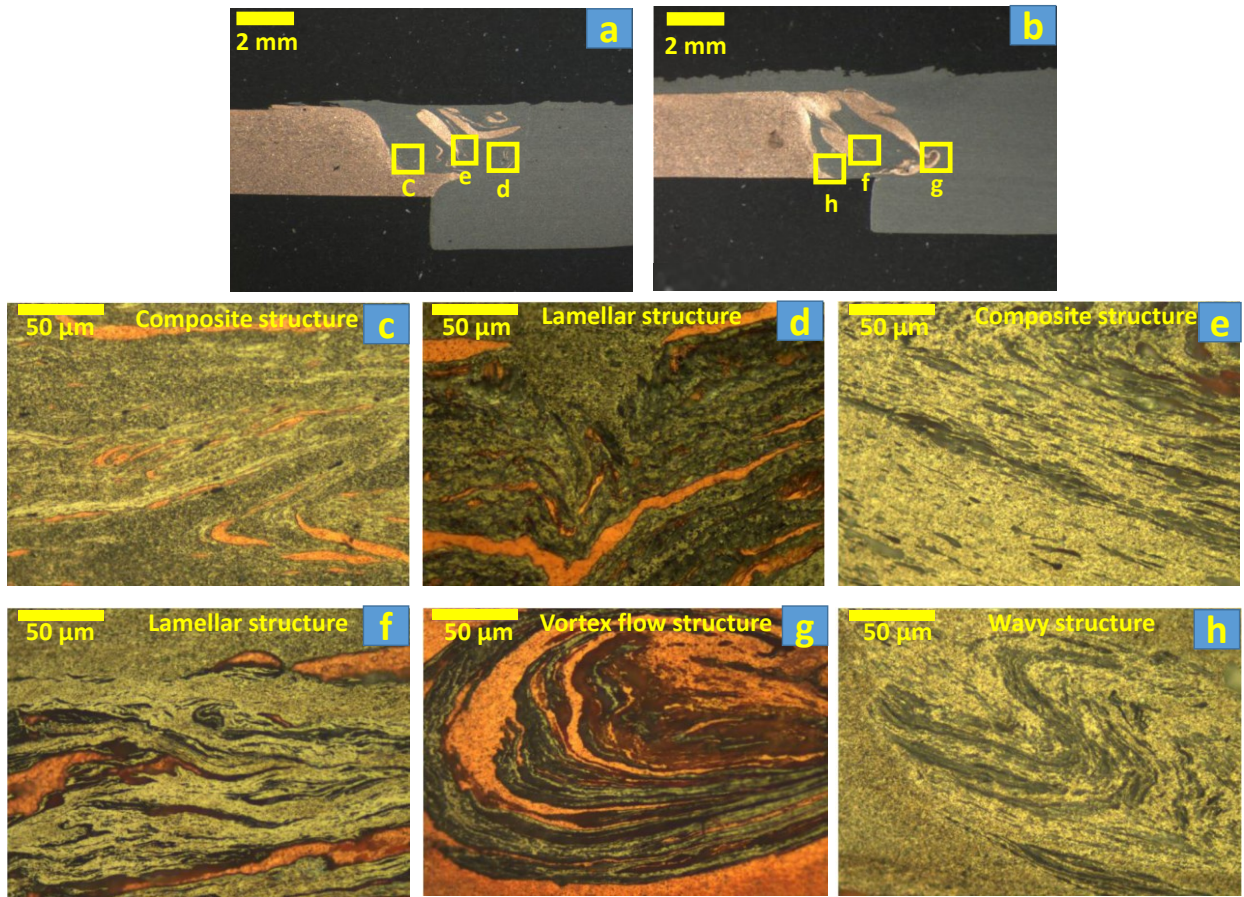
Figure 4 Various flow patterns in a) S3 b) S4 c) S3 d) S3 e) S3 f) S4 g) S4 h) S4

Because the welds are performed without offsets, participation of both the materials in the weld zone remains equal, which contradicts the statement that most of the weld lies in the Al section in offset condition [37]. However, a little increase in the volume of Al is recorded due to the availability of an additional volume of Al, induced by the cross-sectional adjustment of materials in the case of Cu at the middle and bottom positions. The defect-free and improved material mixing in the weld zone leads to enhanced joint efficiency. Small Cu particles make the mixing process easier with Al and thus lead to strong metallurgical bonding in the stir zone. Since the proper material mixing and acceptable defects are only possible for samples S3 and S4, the weld zone's mixed region and root defects are analyzed, as shown in fig. 5. According to Shankar et al., the material distribution in the Al-Cu weld is classified into three different categories partially distributed, uniform, and non-uniform. This uniform distribution of material results in composite structure and thus leads to the increment in tensile strength [28]. Similarly, Esmaeili et al. claimed that the lamellar composite structure increases the tensile strength and vice versa [37]. There are

two different types of Cu material distribution obtained in the weld area; in the first type, the size of the Cu particle seems to be uniform, whereas the second type of distribution consists of varying sizes of the Cu particle in the weld zone. The fig. 5a shows the distribution of Cu particles in sample S3, whereas fig. 5b depicting the Cu distribution in sample S4. The enlarged view of the bigger Cu fragments shows a layered structure that acts as the strengthening mechanism, as shown in fig. 5c.

The most prevalent problems in the practical FSW process are root flaws, which can emerge near the bottom of the weld and are detrimental to weld quality. Several methods have been used to eliminate these defects. Ji et al. used a half screw pin and tapered flute pin to remove the defects as it increases the material velocity at the bottom of the weld [38]. Santos et al. claimed that the reason for the root flaws is insufficient viscoplastic material flow below the probe tip, and these flows can be eliminated by the electrical joule effect, which improves materials viscoplasticity in that region [39]. Fig. 5d and 5e represent the roots of the weld S3 and S4. The root of sample S3 is defect-free, whereas the S4 has flaws at the root. Since the straight penetration restricts the penetration of the tool in the weld zone in the case of S3 compared to sample S4. Therefore, a thicker hook is observed in the case of sample S3 comparatively. The thicker hook in the root area provides support to the tool, thus retaining the material's movement at the root. The upward movement of the Cu material at the bottom of the weld can be easily identified, which shows the movement of material at the bottom. On the other hand, the hook formed at the root of sample S4 is thinner comparatively. The thinner hook at the bottom deforms and creates a gap below the pin and thus leading to flaws.
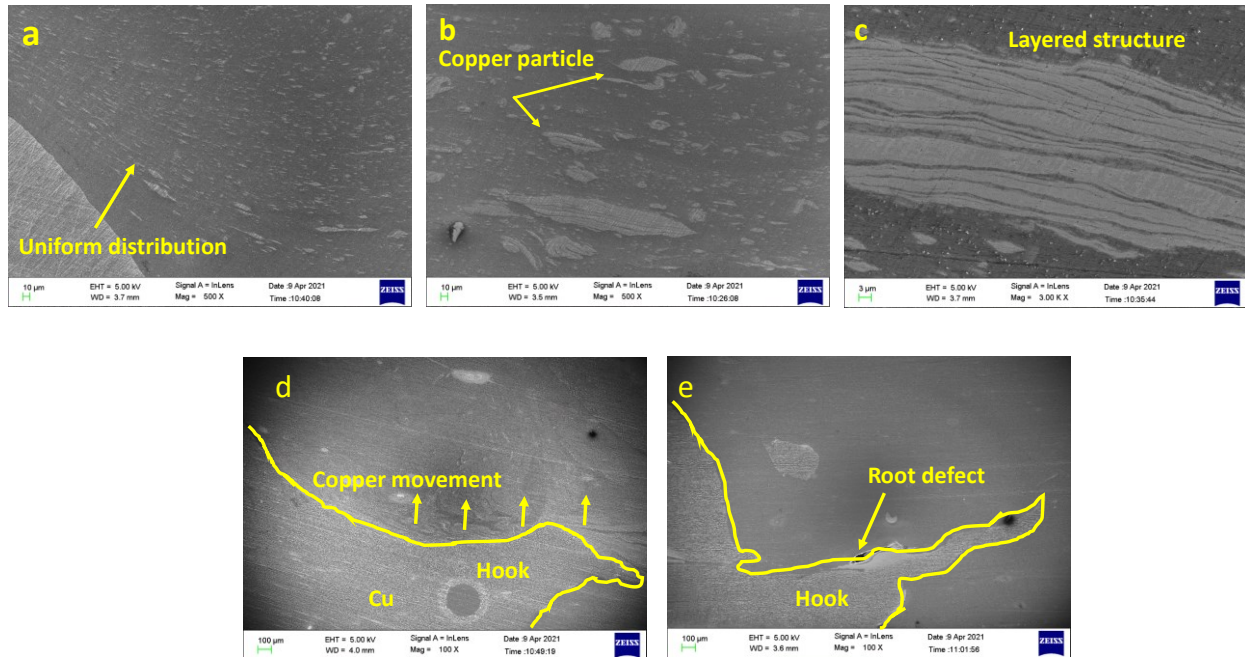
Figure 5 *Microstructural analysis of sample a) S3 b) S4 c) S4 d) S3 e) S4*

The EBSD orientation maps, grain size diameter, and grain boundary rotation angle of different zones such as Al base metal, Cu base metal, stir zone, and interface region of sample S3 is given in figures 7, 8, and 9, respectively. The different images of the fig 7, fig 8, and fig 9 are correspond to the different zones of sample S3, indicted as a, b, c, and d in fig. 6. Fig. 7a and 7b represent the Al and Cu base metal grains, respectively. The grains of the Al base metal are elongated along the rolling direction, whereas Cu has deformed and twin grains. The average grain size of the Al base metal and Cu base metal is 22.25 and 13.73 microns (fig 8a and 8b), respectively, and it can be again confirmed from fig 7a and 7b.with subgrains. The rotating tool's intense plastic strain and heat input substantially impact the microstructural evolution of grains in the stir zone (SZ). The dislocation glide triggered by continuous strain causes the gradual relative rotation of adjacent sub-grains in the initial grains with low-angle borders [40]. The combination of high temperature and constant plastic deformation accelerates the continuous rotation of sub-grains, resulting in the transformation of low-angle grain boundaries (LAGBs) into high angle grain boundaries (HAGBs). The development of refined recrystallized grains within SZ as a result of strong plastic deformation and frictional heating is frequently assumed to be continuous dynamic recrystallization. Initially, recrystallized grains in SZ during welding are very small, with diameters of tens or hundreds of nanometers, but they will grow to be several micrometers due to

the high temperature produced mostly by weld heat input [41]. Fig. 7c and 7d represent the refined grains of the stir, and the interfacial zone corresponds to the points c and d in fig.6. The average grain size of the different zones is smaller than the base metals, which are 11.37 and 1.32 microns for the stir zone and interfacial region, respectively. There is a non-indexed region in the interface, as shown in fig.7d, caused by the severe deformation by the pin. A similar non-indexed region was also reported by Vyas et al. in continuous friction welding of Cu and steel [42].
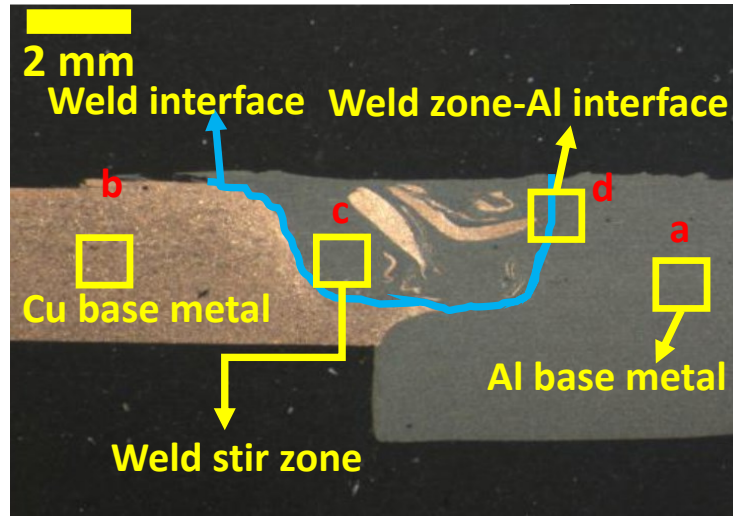

Figure 6 *Position of different zones used for orientation maps, grain size diameter and grain orientation angle of sample S3*
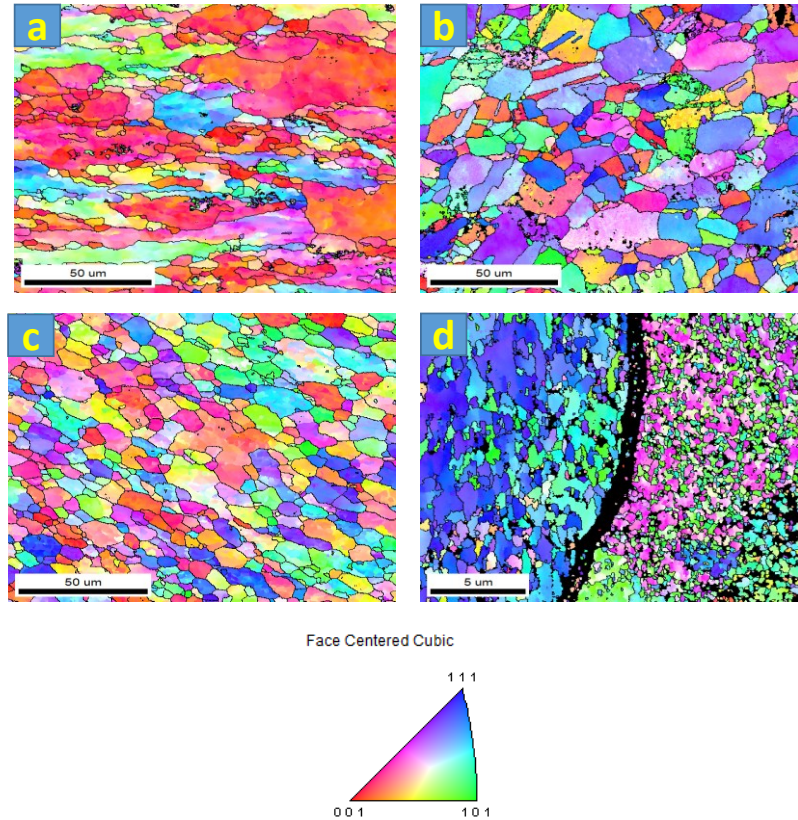
Figure 7 *Orientation map (sample S3) of the zone a) Al base metal b) Cu base metal C) Stir zone d) Al interface region*

Fig. 8 depicts distribution, average (AVG), and standard deviation of grain size in Al base metal (fig. 8a), Cu base metal (fig. 8b), stir zone (fig. 8c), and interfacial region (fig 8d) of sample S3 respectively correspond to the points a, b, c and d as indicated in fig. 6. A larger average grain size of 22.25 micron and a standard deviation of 15.18 micron show a variety of grain sizes in Al base metals. Similarly, Cu base metal also has a larger average grain size of 13.73 microns and a standard deviation of 7.79 microns, indicating that the variance in grain size diameter is less in comparison. On the other hand stir zone (SZ) has more refined grain due to the intense plastic deformation and temperature generation. The average grain size and standard deviation were reduced to 11.37 microns and 6.17 microns, respectively. The interface region has the finest grain size, which indicates that this region experiences severe deformation. The interface region has an average grain diameter of 1.32 microns and a standard deviation of 1.13 microns, which indicates uniform grain in the interface region.
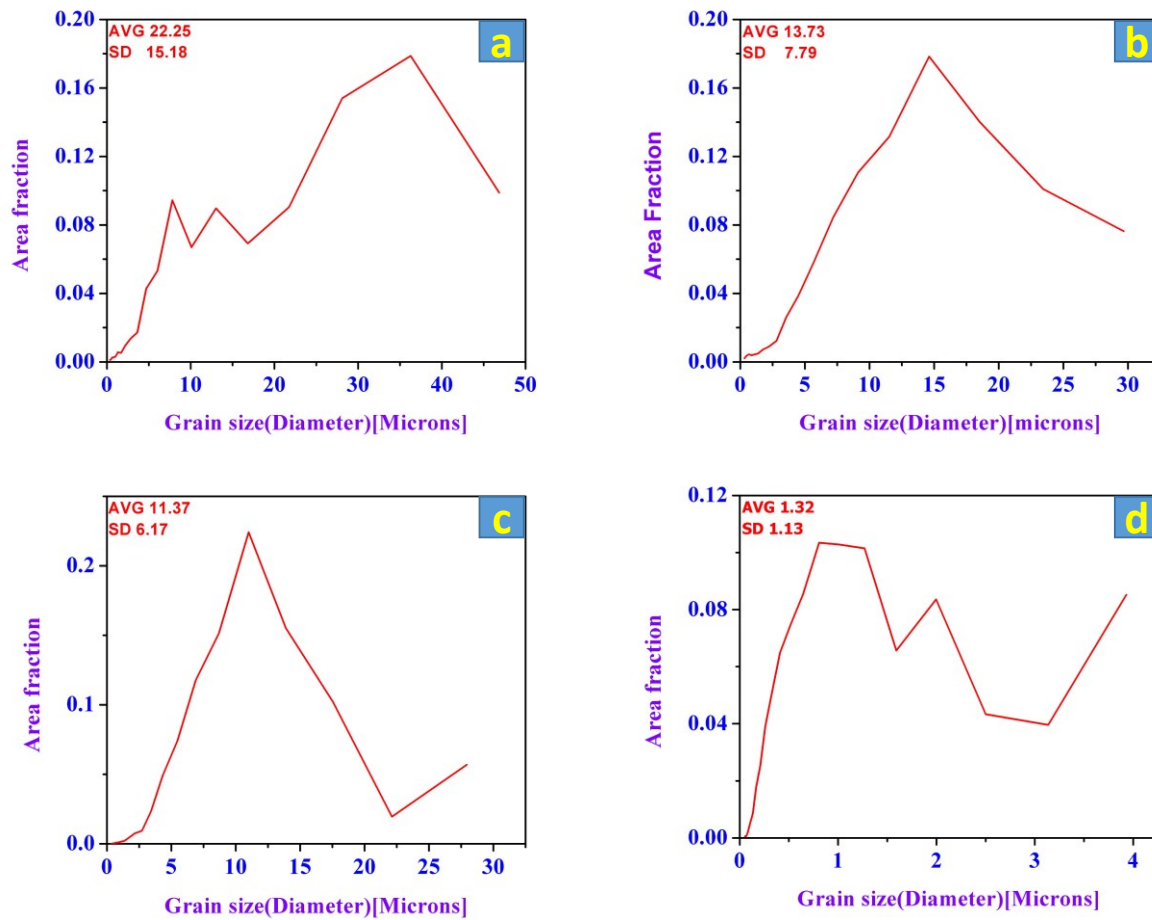
14

Figure 8 *Grain size diameter (sample S3) of zone a) Al base metal b) Cu base metal c) Stir zone d) Al interface*

Fig. 9 represents the boundary rotation angle of Al base metal (fig. 9a), Cu base metal (fig. 9b), stir zone (fig. 9c), and interfacial region (fig 9d), of sample S3 respectively correspond to the points a, b, c and d as indicated in fig. 6. Boundary rotation angle between 1° to 15° was deemed as LAGBs, whereas angle higher than 15° considered as HAGBs. As discussed above, high temperature combined with continuous plastic deformation promotes the continuous rotation of sub-grains, resulting in the transformation of LAGBs into HAGBs. The FSW process significantly changes the misorientation of the grains. Fig 9c shows the significant improvement in the HAGBs after the FSW process. However, the interfacial region shows an increment in the LAGBs due to dynamic recrystallization. The big grains of Al alloy are completely converted into refined grains due to the recrystallization. The right part of the non-indexed region in fig 9d shows the thermo-mechanical affected zone. This zone also experiences high heat and plastic deformation, leading

to the recrystallization of the Al alloy due to the cyclic impact of tool pin. The thermo-mechanical affected zone is also rich in LAGBs.
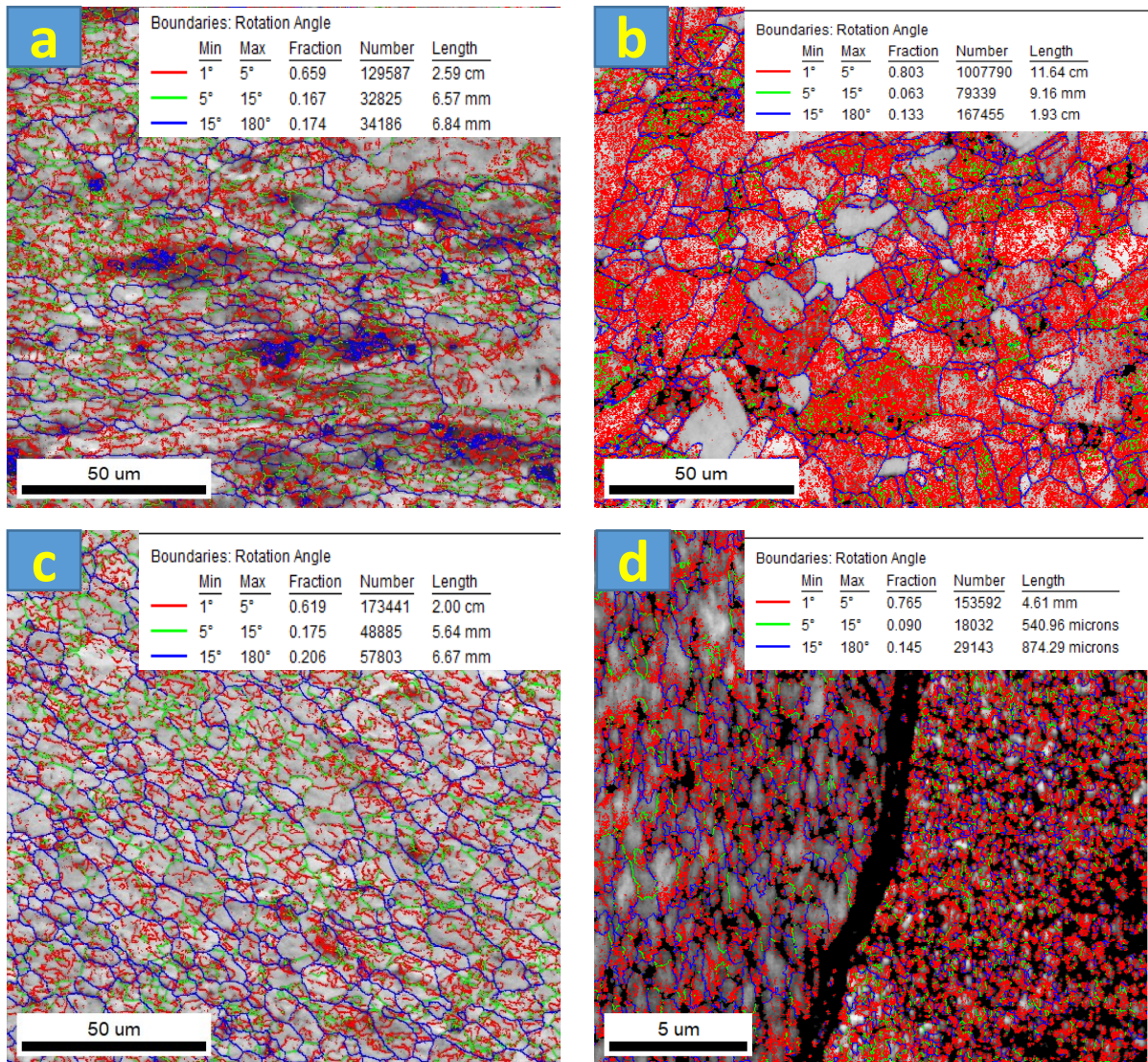

Figure 9 *Boundaries rotation angle (sample S3) of zone a) Al base metal b) Cu base metal c) Stir zone d) Al interface*
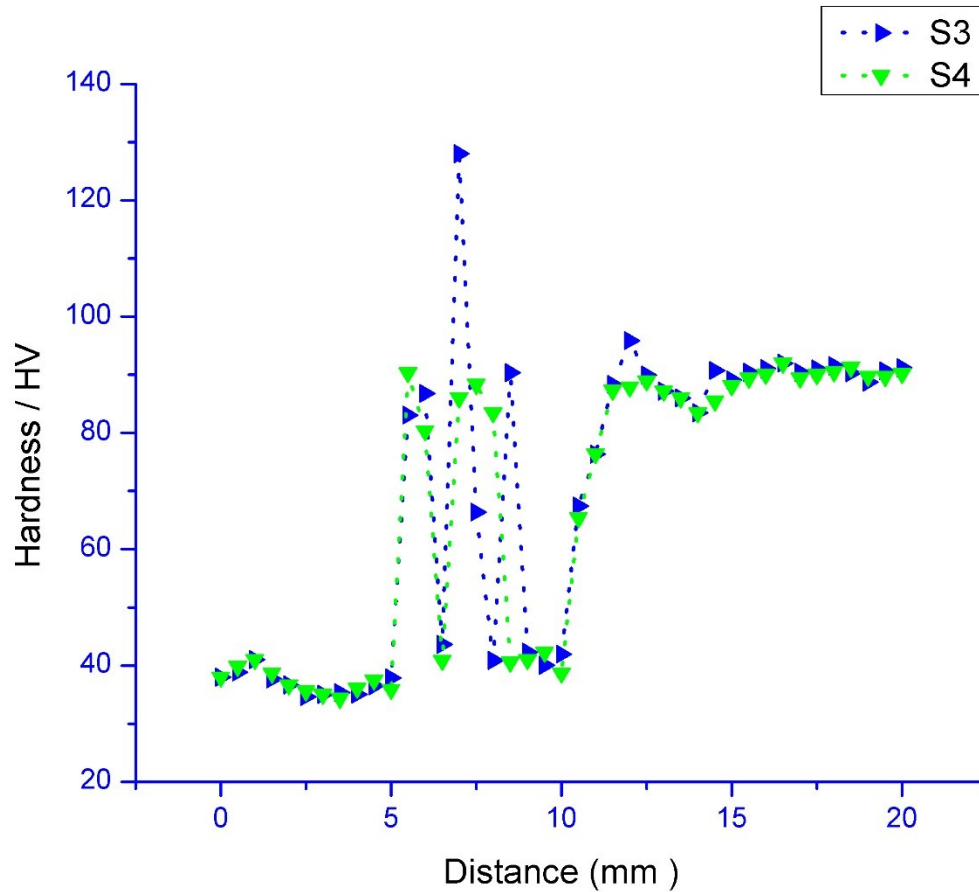
3.3. Micro-hardness analysis

Figure 10 *Micro-hardness distribution of Al-Cu FSWed specimen*

The micro-hardness distribution of samples S3 (Cu at the middle and horizontal bed) and S4 (Cu at the middle and inclined bed) was assessed along the middle part of the transverse cross-section, as shown in fig. 10. The average micro-hardness of the base Al alloy was 40HV, whereas the average micro-hardness of Cu was 90HV. An almost similar trend was observed in different sections of both the samples S3 and S4. However, there is a variation in the weld zone's micro-hardness, representing an inhomogeneous distribution of the Cu particles in the weld nugget. These Cu particles can be found in either fine or coarse fragments. The maximum hardness of 128 HV was obtained in the weld nugget due to the Al solid solution and IMCs in the mixed layer, making

it the hardest spot along the cross-section. The minimum micro-hardness is between the positions 2 mm to 3.5 mm from the extreme ends towards Al alloys. The reduction in the hardness value claims the presence of HAZ along the Al alloy, caused by the dissolution of precipitates. Moreover, the micro-hardness of both the Al and Cu alloys along the HAZ region was lower than the base metal because of the grain coarsening caused by the frictional heating [43].

3.4. Strength of the joint
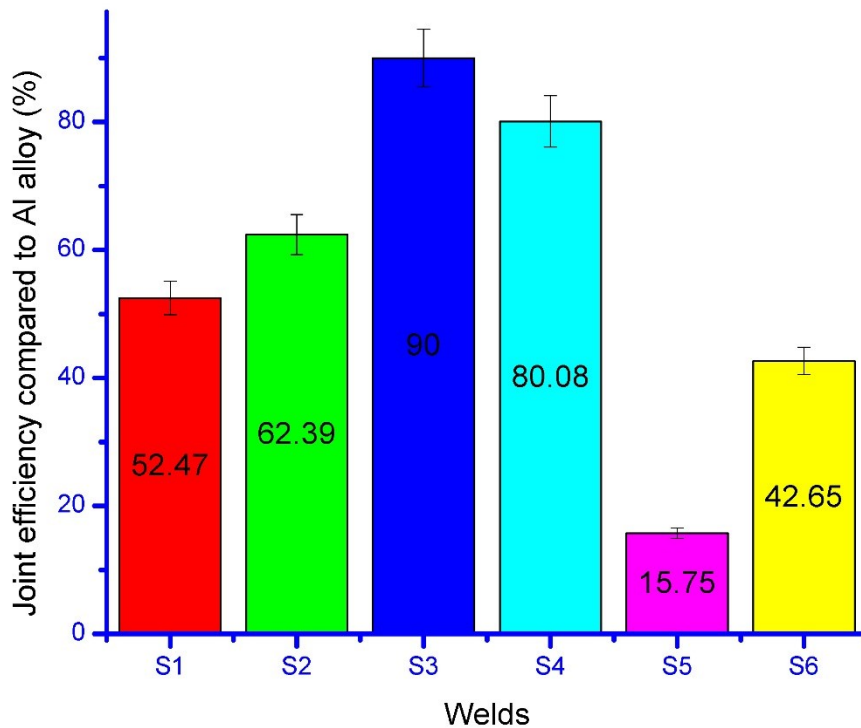
Figure 11 *Percentage strength compared to Al base metal*

Tensile test for different samples prepared at different conditions and corresponding welds' joint efficiency compared to the base Al alloy is shown in fig. 11. In any dissimilar weld, the strength is always compared to the weaker base metal. The maximum tensile strength of 101.7 MPa was obtained with the S3 (Cu at middle position and horizontal bed condition), which is 90% of the Al base metal, whereas the minimum tensile strength of 17.8 MPa was achieved with sample

S5 (Cu at bottom position and horizontal bed condition) which is only 15.75% of the base Al alloy. The UTS obtained with S5 is quite low comparatively and not acceptable for any industrial application. Moreover, the tensile strength obtained in the case of friction stir welded Al-Cu alloys is always less than the base Al alloy, which is 113 MPa in the current experiment. Both welds, horizontal and inclined bed conditions, show a tensile strength of 52.47% and 62.39%, while the Cu was placed at the top position, which is lower than the several literatures. The reason for this reduced strength is the formation of cracks, root defects, and bulk Cu particles, which is very common for weld produced without offsets. Similarly, samples S5 and S6 prepared with Cu at the bottom position show the lowest joint efficiency of 15.75% and 42.65% due to improper shoulder alignment and lack of plunge force due to the unique joint configuration and a huge amount of defects. On the other hand, opposite to Cu at top and bottom, middle position welds shows a joint efficiency of 90% and 80.08% for sample S3 and S4 that are reflecting a significant improvement in the strength which is almost impossible with the welds without offsets. Elimination of cracks, proper alignment of shoulder, and flash reduction improve joint efficiency.

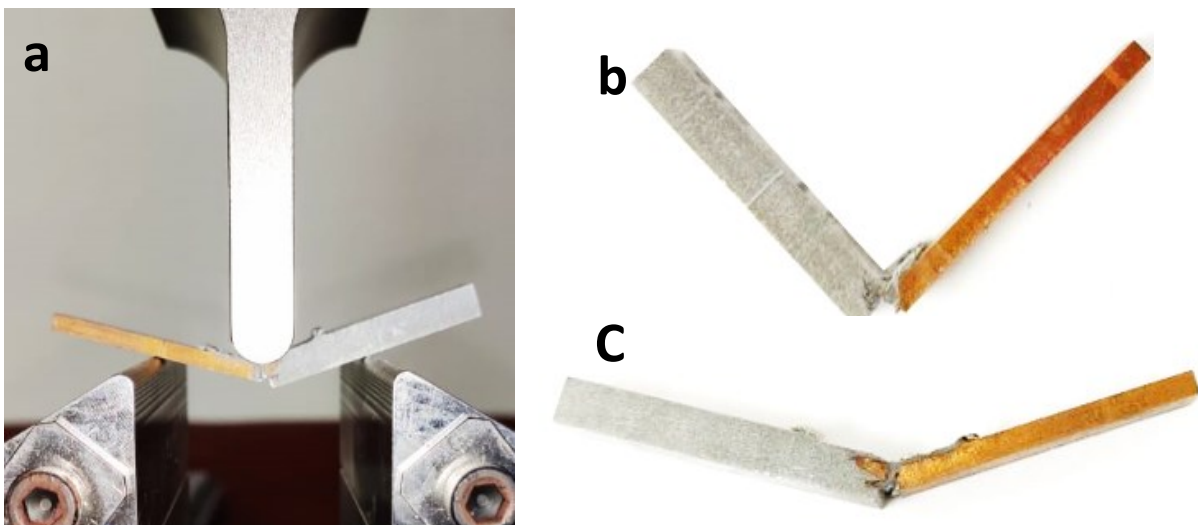### 3.5. Three-point bending test analysis

Figure 12 Three-point flexural test for a) Test set-up b) S3 c) S4

Fig. 12 shows the root bend specimens in the three-point bending test. Since only the samples S3 and S4 have demonstrated an acceptable quality of joint strength. Therefore, only these samples

are selected for the bending test analysis. However, it has been discussed earlier that both the welds are performed in Cu at the middle position with and without inclination angle. The bottom part of the specimen experiences a tensile force, whereas the top section experiences a compressive force. The sample S3 and S4 shows bending angle of 93˚ and 35˚, respectively. In both the samples, cracks were initiated at the center. In sample S3, the crack stuck at the initiation point, whereas it propagated through the Cu interface of the weld zone for sample S4. Since Al is the dominating member in sample S3, thus, due to its better ductility, it has shown an improved bending angle, whereas, due to the brittle nature of the interface zone, it propagates through the weld zone in S4.
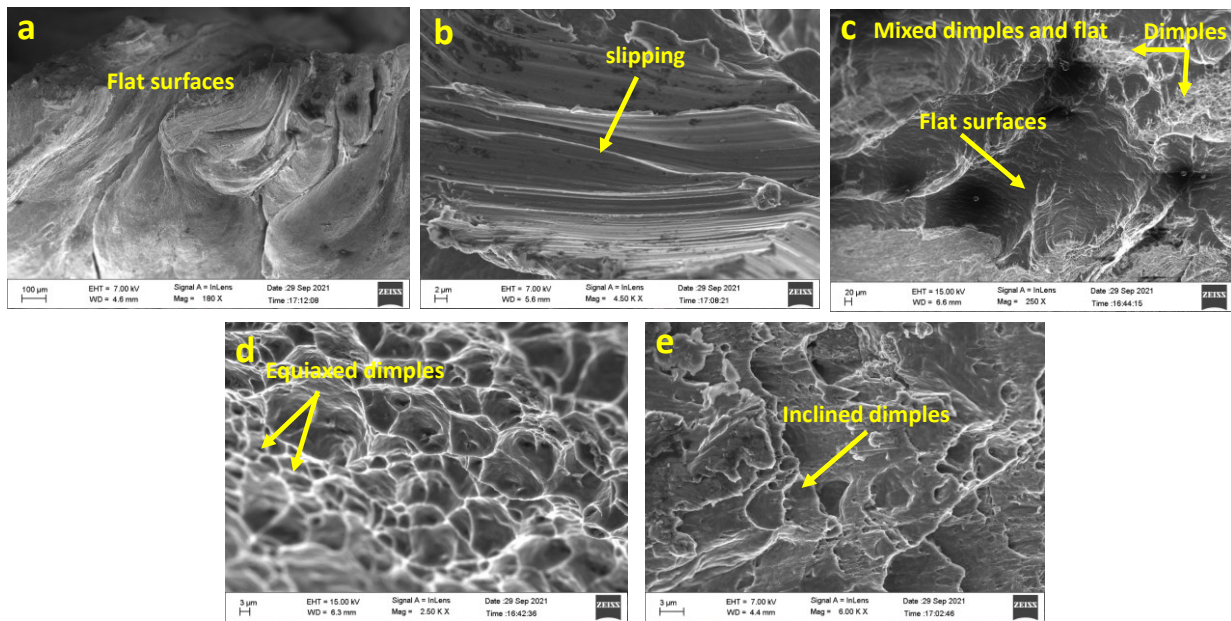
.

3.6.   *Fracture surface*

Figure 13 *Fracture surface of different FSWed Al-Cu sample a) S1 b) S1 c) S4 d) S3 e) S4*

The microscopic fractography reveals a lot about the nature of the fracture surface. Fig. 13 represents the FESEM image of fractured surfaces of different Al-Cu welded samples. The fracture surface of the weld zone can be divided into three types flat surfaces, mixed regions of dimples and flat surfaces, and only dimples. Fig. 13a demonstrates only the cleavages and flat surfaces, which signifies a brittle fracture due to voluminous Cu particles. Slipping of material is also a common feature of these types of failure, as depicted in fig 13b. However, these types of fracture surfaces also indicate the absence of material mixing in the weld zone. On the other hand, mixed

flat and dimples demonstrate a partial mixing and relatively small Cu fragments, as shown in fig. 13c. This is the most common type of feature in the FSWed Al and Cu alloys because the complete mixing of materials is not possible since the welds are performed without offsets. Fig 13 d and e represent the two different types of dimples in samples S3 and S4, respectively. The dimples can be divided into two categories deep and shallow. The deep dimples indicate a higher amount of force before fracture than the shallow one [44].

Similarly, deep dimples also represent an excellent metallic bonding between the materials. However, the dimples in fig.13e are inclined compared to fig 13d, which represents the presence of shear force also.

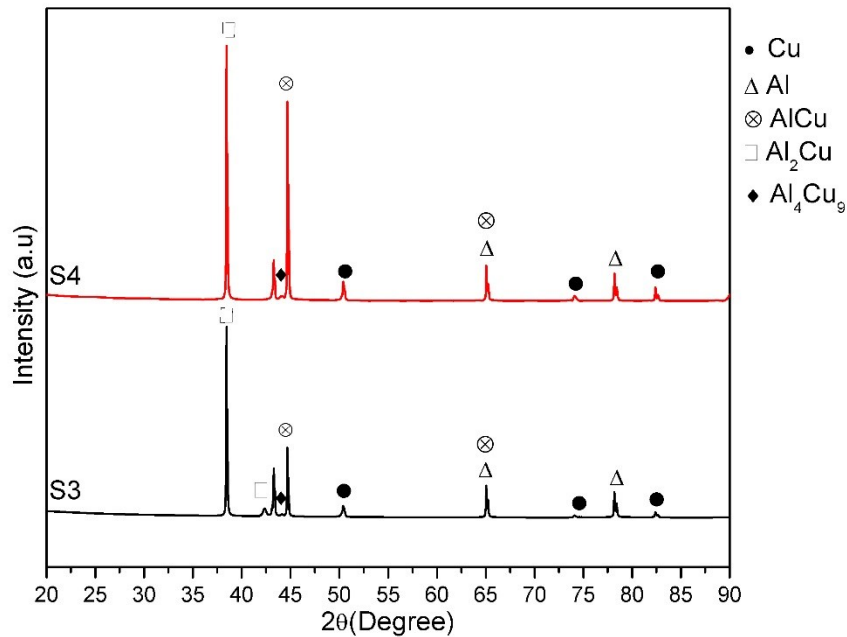### 3.7.   Intermetallic phases

Figure 14 XRD analysis of sample S3 and S4

To identify the phases present in the stir zone, an XRD analysis was conducted on the cross-sections. The XRD patterns of two typical defect-free S3 and S4 joints are shown in fig. 14. Al_2Cu, AlCu, and Al_4Cu_9 are the three most common types of intermetallics formed in the weld zone.

Al_2Cu phases form at 150 ˚C, while Al_4Cu_9 phases form at 350˚C. When the intermetallic phase reaches a thickness of 10μm, the bond strength begins to decline sharply[15]. Since all the experiments are performed without offsets, the improved stirring and mixing of the bulk Cu particle leads to the formation of intermetallic compounds in the weld zone. Among the many reasons, the formation of intermetallics is also a cause that contributes for reducing the joint strength in dissimilar friction stir welding of Al-Cu. These intermetallics are the invisible participants, which restricts the joint strength to match the strength of the Al alloy in dissimilar Al-Cu weld.

4.   *Conclusions*

Friction stir welding of dissimilar Al-Cu alloys with different thicknesses, wherein Cu was placed at different positions (i.e., at the top, middle and bottom) with respect to the Al alloy and without the offsets, were studied in detail. The current observations lead to the following conclusions:

1. In both the horizontal and inclined bed conditions, the defect-free and sound joints are only possible while the Cu was placed at middle positions due to the availability of additional Al volume. This extra volume of Al eliminates the surface channeling and defects, which was prevalent in the case of Cu at the top positions.

2. The welding of Cu at the bottom position is completely impossible in horizontal bed conditions because of the improper tool movement and difficulty in keeping material under the shoulder. On the other hand, the inclined bed condition results in slightly improved weld comparatively but remains to be inadequate.

3. The maximum tensile strength of 101.7 MPa was obtained with S3 (Cu at middle position and horizontal bed condition), which is 90% of the base Al alloy, whereas the minimum strength of 17.8 MPa was achieved with the sample S5 (Cu at bottom position and horizontal bed condition). The cause for the maximum strength is appropriate mixing of material and defect-less joints.

4. The three-point bending test presents a bending angle of 93˚ and 35˚ for samples S3 and S4, which indicates that the sample S3 shows the maximum tensile strength as well as the most favorable bending angle.

5. The hardness curve is asymmetrical with respect to the weld centerline. The minimum micro-hardness of 34.35 HV was obtained in HAZ along the Al side, whereas the maximum micro-hardness of 128 HV was obtained in the Al-Cu mixed zone. The reason for this improved

hardness is the formation of intermetallics in the mixed region. The most common intermetallics formed in the weld zone are AlCu, Al_2Cu, and Al_4Cu_9.

References

[1]   B. Mvola, P. Kah, J. Martikainen, Welding of dissimilar non-ferrous metals by GMAW processes, International Journal of Mechanical and Materials Engineering. 9 (2014) 1–11. doi:10.1186/s40712-014-0021-8.

[2]   G. İpekoğlu, G. Çam, Effects of initial temper condition and postweld heat treatment on the properties of dissimilar friction-stir-welded joints between AA7075 and AA6061 aluminum alloys, Metallurgical and Materials Transactions A: Physical Metallurgy and Materials Science. 45 (2014) 3074–3087. doi:10.1007/s11661-014-2248-7.

[3]   A. Elrefaey, M. Takahashi, K. Ikeuchi, PRELIMINARY INVESTIGATION OF FRICTION STIR WELDING ALUMINIUM / COPPER LAP JOINTS, Welding in the World. 49 (2006) 93–101.

[4]   A. Heidarzadeh, S. Mironov, R. Kaibyshev, G. Çam, A. Simar, A. Gerlich, F. Khodabakhshi, A. Mostafaei, D.P. Field, J.D. Robson, A. Deschamps, P.J. Withers, Friction stir welding/processing of metals and alloys: A comprehensive review on microstructural evolution, Progress in Materials Science. 117 (2020) 100752. doi:10.1016/j.pmatsci.2020.100752.

[5]   G. Çam, G. İpekoğlu, Recent developments in joining of aluminum alloys, International Journal of Advanced Manufacturing Technology. 91 (2017) 1851–1866.

[6]   G. Çam, S. Mistikoglu, M. Pakdil, Microstructural and mechanical characterization of friction stir butt joint welded 63% Cu-37% Zn brass plate, Welding Journal (Miami, Fla). 88 (2009).

[7]   T. Küçükömeroğlu, S.M. Aktarer, G. İpekoğlu, G. Çam, Microstructure and mechanical properties of friction-stir welded St52 steel joints, International Journal of Minerals, Metallurgy and Materials. 25 (2018) 1457–1464. doi:10.1007/s12613-018-1700-x.

[8]   T. Küçükömeroğlu, S.M. Aktarer, G. İpekoğlu, G. Cam, Mechanical properties of friction stir welded St 37 and St 44 steel joints, Materials Testing. 60 (2018) 1163–1170. doi:10.3139/120.111266.

[9]   T. Küçükömeroğlu, S.M. Aktarer, G. Çam, Investigation of mechanical and microstructural properties of friction stir welded dual phase (DP) steel, IOP Conference Series: Materials Science and Engineering. 629 (2019). doi:10.1088/1757-899X/629/1/012010.

[10]   G. Çam, Friction stir welded structural materials: Beyond Al-alloys, International Materials

Reviews. 56 (2011) 1–48. doi:10.1179/095066010X12777205875750.

[11]   G. Ipekoglu, S. Erim, G. Cam, Investigation into the influence of post-weld heat treatment on the friction stir welded AA6061 Al-Alloy plates with different temper conditions, Metallurgical and Materials Transactions A: Physical Metallurgy and Materials Science. 45 (2014) 864–877. doi:10.1007/s11661-013-2026-y.

[12]   G. Çam, G. Ipekoğlu, H. Tarık Serindağ, Effects of use of higher strength interlayer and external cooling on properties of friction stir welded AA6061-T6 joints, Science and Technology of Welding and Joining. 19 (2014) 715–720. doi:10.1179/1362171814Y.0000000247.

[13]   F. Bakhtiari, A. Ali, S. Seyyed, E. Mirsalehi, Dissimilar Joining of Pure Copper to Aluminum Alloy via Friction Stir Welding, Acta Metallurgica Sinica (English Letters). 31 (2018) 1183–1196. doi:10.1007/s40195-018-0741-5.

[14]   K.P. Mehta, V.J. Badheka, Effects of Tilt Angle on Properties of Dissimilar Friction Stir Welding Copper to Aluminum, Materials and Manufacturing Processes. (2014) 37–41. doi:10.1080/10426914.2014.994754.

[15]   S. Celik, R. Cakir, Effect of Friction Stir Welding Parameters on the Mechanical and Microstructure Properties of the, Metals. 6 (2016). doi:10.3390/met6060133.

[16]   A.O. Al-roubaiy, S.M. Nabat, Experimental and theoretical analysis of friction stir welding of Al – Cu joints, International Journal of Advanced Manufacturing Technology. 71 (2014) 1631–1642. doi:10.1007/s00170-013-5563-z.

[17]   M. Felix Xavier Muthu, V. Jayabalan, Effect of pin profile and process parameters on microstructure and mechanical properties of friction stir welded Al-Cu joints, Transactions of Nonferrous Metals Society of China (English Edition). 26 (2016) 984–993. doi:10.1016/S1003-6326(16)64195-X.

[18]   E.T. Akinlabi, A. Andrews, S.A. Akinlabi, Effects of processing parameters on corrosion properties of dissimilar friction stir welds of aluminium and copper, Transactions of Nonferrous Metals Society of China. 24 (2014) 1323–1330. doi:10.1016/S1003-6326(14)63195-2.

[19]   N.A. Muhammad, C.S. Wu, Ultrasonic vibration assisted friction stir welding of aluminium alloy and pure copper, Journal of Manufacturing Processes. 39 (2019) 114–127. doi:10.1016/j.jmapro.2019.02.011.

[20]   N.A. Muhammad, C. Wu, Evaluation of capabilities of ultrasonic vibration on the surface , electrical and mechanical behaviours of aluminium to copper dissimilar friction stir welds, International Journal of Mechanical Sciences. 183 (2020) 105784. doi:10.1016/j.ijmecsci.2020.105784.

[21]   I. Galvão, J.C. Oliveira, A. Loureiro, D.M. Rodrigues, Formation and distribution of brittle structures in friction stir welding of aluminium and copper : Influence of shoulder geometry, Intermetallics. 22 (2012) 122–128. doi:10.1016/j.intermet.2011.10.014.

[22]   K.P. Mehta, V.J. Badheka, Hybrid approaches of assisted heating and cooling for friction stir welding of copper to aluminum joints, Journal of Materials Processing Technology. 239

(2017) 336–345. doi:10.1016/j.jmatprotec.2016.08.037.

[23]   L.I. Xia-wei, Z. Da-tong, Q.I.U. Cheng, Z. Wen, Microstructure and mechanical properties of dissimilar pure copper / 1350 aluminum alloy butt joints by friction stir welding, Transactions of Nonferrous Metals Society of China. 22 (2012) 1298–1306. doi:10.1016/S1003-6326(11)61318-6.

[24]   H. Okamura, K. Aota, Joining of dissimilar materials with friction stir welding, Welding International. 18 (2004) 852–860. doi:10.1533/wint.2004.3344.

[25]   G. Çam, V. Javaheri, A. Heidarzadeh, Advances in FSW and FSSW of dissimilar Al-alloy plates, Journal of Adhesion Science and Technology. 0 (2022) 1–33. doi:10.1080/01694243.2022.2028073.

[26]   W. Hou, L.H. Ahmad Shah, G. Huang, Y. Shen, A. Gerlich, The role of tool offset on the microstructure and mechanical properties of Al/Cu friction stir welded joints, Journal of Alloys and Compounds. 825 (2020) 154045. doi:10.1016/j.jallcom.2020.154045.

[27]   P. Xue, D.R. Ni, D. Wang, B.L. Xiao, Z.Y. Ma, Effect of friction stir welding parameters on the microstructure and mechanical properties of the dissimilar Al – Cu joints, Materials Science and Engineering A. 528 (2011) 4683–4689. doi:10.1016/j.msea.2011.02.067.

[28]   S. Shankar, P. Vilaça, P. Dash, S. Chattopadhyaya, S. Hloch, Joint strength evaluation of friction stir welded Al-Cu dissimilar alloys, Measurement. 146 (2019) 892–902. doi:10.1016/j.measurement.2019.07.019.

[29]   S.M.O. Tavares, J.F. dos Santos, P.M.S.T. de Castro, Friction stir welded joints of Al-Li Alloys for aeronautical applications: Butt-joints and tailor welded blanks, Theoretical and Applied Fracture Mechanics. 65 (2013) 8–13. doi:10.1016/j.tafmec.2013.05.002.

[30]   Y. Hovanski, P. Upadhyay, J. Carsley, T.O.M. Luzanski, B. Carlson, M. Eisenmenger, A. Soulami, D. Marshall, B. Landino, S. Hartfield-wunsch, High-Speed Friction-Stir Welding to Enable Aluminum Tailor-Welded Blanks, The Journal of The Minerals, Metals & Materials Society. 67 (2015) 1045–1053. doi:10.1007/s11837-015-1384-x.

[31]   M.B. Silva, M. Skjoedt, P. Vilaça, N. Bay, P.A.F. Martins, Single point incremental forming of tailored blanks produced by friction stir welding, Journal of Materials Processing Technology. 209 (2009) 811–820. doi:10.1016/j.jmatprotec.2008.02.057.

[32]   L. Fratini, G. Buffa, R. Shivpuri, Improving friction stir welding of blanks of different thicknesses, Materials Science and Engineering A. 459 (2007) 209–215. doi:10.1016/j.msea.2007.01.041.

[33]   E. Kamalvand, A. Jabbari, M.R. Sheykholeslami, S. Mazdak, R. Beygi, S. Mohammadi, Effect of friction stir welding parameters on the deep drawing of tailor-welded blanks (TWBs), CIRP Journal of Manufacturing Science and Technology. 33 (2021) 91–99. doi:10.1016/j.cirpj.2021.02.011.

[34]   M. Parente, R. Safdarian, A.D. Santos, A. Loureiro, P. Vilaca, R.M.N. Jorge, A study on the formability of aluminum tailor welded blanks produced by friction stir welding, International Journal of Advanced Manufacturing Technology. 83 (2016) 2129–2141. doi:10.1007/s00170-015-7950-0.

[35]   M. Habibi, R. Hashemi, M. Fallah Tafti, A. Assempour, Experimental investigation of mechanical properties, formability and forming limit diagrams for tailor-welded blanks produced by friction stir welding, Journal of Manufacturing Processes. 31 (2018) 310–323. doi:10.1016/j.jmapro.2017.11.009.

[36]   R. Beygi, M. Zarezadeh Mehrizi, A. Akhavan-Safar, S. Safaei, A. Loureiro, L.F.M. da Silva, Design of friction stir welding for butt joining of aluminum to steel of dissimilar thickness: heat treatment and fracture behavior, International Journal of Advanced Manufacturing Technology. 112 (2021) 1951–1964. doi:10.1007/s00170-020-06406-3.

[37]   A. Esmaeili, H.R.Z. Rajani, M. Sharbati, M.K.B. Givi, M. Shamanian, The role of rotation speed on intermetallic compounds formation and mechanical behavior of friction stir welded brass / aluminum 1050 couple, Intermetallics. 19 (2011) 1711–1719. doi:10.1016/j.intermet.2011.07.006.

[38]   S. Ji, J. Xing, Y. Yue, Y. Ma, L. Zhang, S. Gao, Design of Friction Stir Welding Tool for Avoiding Root Flaws, Materials. 6 (2013) 5870–5877. doi:10.3390/ma6125870.

[39]   T.G. Santos, R.M. Miranda, P. Vilac, Friction Stir Welding assisted by electrical Joule effect, Journal of Materials Processing Technology. 214 (2014) 2127–2133. doi:10.1016/j.jmatprotec.2014.03.012.

[40]   P.L. Threadgill, A.J. Leonard, H.R. Shercliff, P.J. Withers, Friction stir welding of aluminium alloys, International Materials Reviews. 54 (2009) 49–93. doi:10.1179/174328009X411136.

[41]   S. Lin, J. Tang, S. Liu, Y. Deng, H. Lin, H. Ji, L. Ye, X. Zhang, Effect of Travel Speed on Microstructure and Mechanical Properties of FSW Joints for Al – Zn – Mg Alloy, Materials. 12 (2019).

[42]   H.D. Vyas, K.P. Mehta, V. Badheka, B. Doshi, Microstructure evolution and mechanical properties of continuous drive friction welded dissimilar copper-stainless steel pipe joints, Materials Science and Engineering: A. 832 (2022) 142444. doi:10.1016/j.msea.2021.142444.

[43]   K. Bang, K. Lee, H. Bang, H. Bang, Interfacial Microstructure and Mechanical Properties of Dissimilar Friction Stir Welds between 6061-T6 Aluminum and Ti-6 % Al-4 % V Alloys , Materials Transactions. 52 (2011) 974–978. doi:10.2320/matertrans.L-MZ201114.

[44]   N.Z. Khan, A.N. Siddiquee, Z.A. Khan, Proposing a new relation for selecting tool pin length in friction stir welding process, Measurement: Journal of the International Measurement Confederation. 129 (2018) 112–118. doi:10.1016/j.measurement.2018.07.015.